Jurnal Kejuruteraan 37(6) 2025: 2809-2816
https://doi.org/10.17576/jkukm-2025-37(6)-19

Strain-Stress Behaviour Investigation on Railway Track Based on The FBG Wavelength Shifting: Rectangular Rosette Configuration

Meor Iqram Meor Ahmad[a*], Mohd Afiq Irfan Syauqi[a], Mohd Zaki Nuawi[a], Mohd Sabirin Rahmat[a], Mohd Anas Mohd Sabri[a], Mohd Hafizi Zohari[b] & Aiman Izzuddeen Anuar[c]

[a]*Department of Mechanical & Manufacturing Engineering, Faculty of Engineering and Built Environments Universiti Kebangsaan Malaysia, 43600, UKM Bangi, Selangor, Malaysia*

[b]*Advanced Structural Integrity and Vibration Research (ASIVR), Faculty of Mechanical and Automotive Engineering Technology, Universiti Malaysia Pahang, 26600, Pekan, Pahang, Malaysia*

[c]*Rail Engineering Department, Track Network Maintenance Ampang Line, 5th Mile Jalan Ampang, 68000, Ampang, Selangor, Malaysia*

**Corresponding author: meoriqram@ukm.edu.my*

Received 29 May 2023, Received in revised form 20 June 2025
Accepted 21 July 2025, Available online 30 September 2025

ABSTRACT

One of the main causes of railway track failure is fatigue fracture, particularly in steel materials. Frequent use can compromise the structural integrity of the tracks, making regular monitoring and daily maintenance essential to ensure safe operation. To support effective maintenance, an efficient system must be established to detect early signs of deformation on the railway tracks. The objective of this study is to develop an understanding of the strain-stress behaviour in railway tracks. A Fibre Bragg Grating (FBG) sensor with a Rosette arrangement is used in this investigation to measure strain under both static and dynamic conditions. The Rosette configuration is chosen because it groups two or more FBG sensors together, allowing for the measurement of strain in multiple directions. The FBG sensors are installed 120 metres from the station, specifically at a critical point, to collect strain data. Once the data is obtained, a strain-stress analysis is conducted to assess the strain behaviour of the track. The results show that the principal strain and stress recorded by the sensor mounted at 90° are higher compared to those at 45° and 0°. The average principal strain is 37.3540 με, while the average principal stress is 16.1339 MPa. Implementing an efficient system of this nature can significantly reduce the risk of railway track failure by enabling early prediction and timely intervention.

Keywords: Structural integrity; railway track; FBG Sensors; strain-stress

INTRODUCTION

Railway development is crucial to the local economy and the transportation system in Malaysia (Suhaimi et al. 2024a). Modern transportation systems, particularly those utilizing the latest technology, heavily depend on railways, which play a vital role in transporting passengers and large cargo from industrial sites and factories to commercial destinations. However, with technological advancement comes the challenge of maintenance, especially given the uncertainties associated with railway infrastructure (Cong Du et al. 2020). These uncertainties can pose serious risks to the reliability and safety of railway operations. In response, railway operators are placing greater emphasis on the development of effective monitoring systems and data-driven maintenance strategies. The integration of smart sensing technologies and predictive analytics is becoming more common in efforts to enhance the reliability, efficiency, and sustainability of railway operations.

Weather changes, climate variations, and natural disasters can potentially damage the railway system, affecting infrastructure, operations, cargo, and the security of surrounding areas. These environmental changes can lead to significant physical deterioration of railway tracks (Cong Du et al. 2020). In the absence of an efficient system to detect structural failures on the tracks, accidents may occur, risking passenger lives and causing damage to trains and cargo. Therefore, maintaining railway tracks is a major challenge, as it is essential to ensure that the infrastructure remains free from defects (Tariq et al. 2014).

Engineers and scientists are continually developing new technologies for railway systems to enhance the efficacy and efficiency of electric trains (Nordin et al. 2017). Once technology is developed, the next critical step involves careful maintenance to ensure safety and smooth operation. Non-Destructive Testing (NDT) is a commonly used inspection method in technology and industry to evaluate the characteristics of components or systems without causing damage. In the railway sector, the use of various sensors and methods, such as Acoustic Emission (AE) and Ultrasonic Testing (UT), is widespread. These sensors are employed to detect a wide range of flaws, including near-surface, interior, and surface defects (Amir Falamarzi et al. 2018). At the same time, the need for non-destructive identification of internal flaws is growing (Takayuki et al. 2010). The metal magnetic memory (MMM) technique is also used to analyze crack growth life in mechanical components, where the correlation curve of magnetic flux leakage signals is evaluated to determine the critical value point with respect to the step size (Ahmad et al. 2016)

The Fiber Bragg Grating (FBG) sensor is increasingly regarded as a next-generation measurement tool for railway track condition monitoring, owing to its numerous advantageous properties. These include immunity to electromagnetic interference, resistance to corrosion, ease of sensor multiplexing, and high resolution (Quan et al. 2014). These characteristics make FBG sensors highly suitable for the challenging environmental and operational conditions of railway systems, ensuring reliable and accurate strain measurements over extended periods (Suhaimi et al. 2023 and Suhaimi et al. 2024(b)).

Therefore, this study employs fiber optic sensors—specifically, the latest technology widely used internationally in applications such as railway monitoring. These sensors enable faster data acquisition, with results presented in graphical form for analysis. The system can detect early-stage failures (Velha et al. 2020), highlighting the need for continuous, real-time monitoring and early warning systems for high-speed railway track conditions (Yongjia Zhang et al. 2017). To support this research, comprehensive preparation was undertaken, including the setup of FBG sensors and related systems, to study strain-stress behavior on railway tracks.

METHODOLOGY

PREPARATION AND CALIBRATION

In this study, the Ampang Line railway track was selected as the experimental site due to its high-risk environment and complex physical configuration. The research focuses on the segment between Miharja and Chan Sow Lin stations. Prior to deployment on the railway track, Fiber Bragg Grating (FBG) sensors were prepared and calibrated in the laboratory. The overall methodology is illustrated in Figure 1. The FBG system setup, including the required equipment, is shown in Figure 2(a). Additionally, a board was designed at a specific angle to facilitate the arrangement of the FBG sensors in a rectangular rosette configuration, as depicted in Figure 2(b).

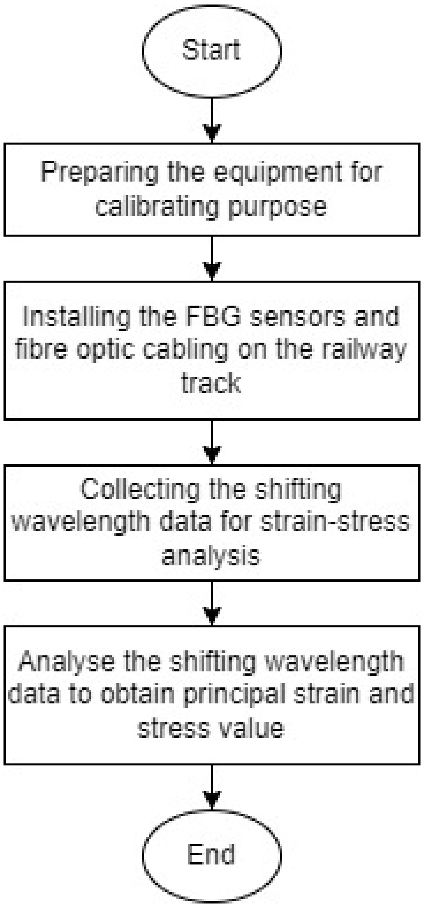

FIGURE 1. Flow chart of the methodology

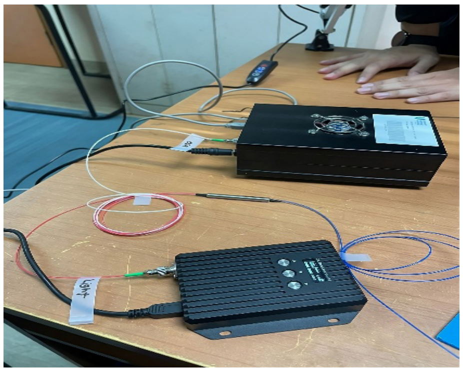

(a)

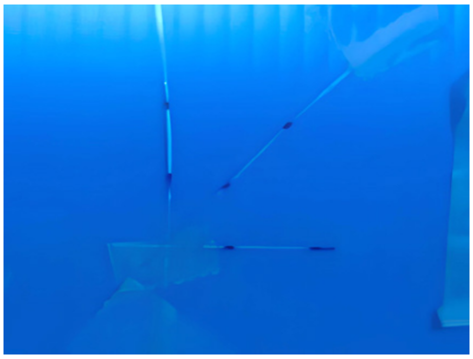

(b)

FIGURE 2. (a) Preparation of FBG sensors in the laboratory (b) Rectangular rosette arrangement

INSTALLATION OF THE FBG SENSORS

Subsequently, the railway surface-particularly at the thermite weld locations-was meticulously cleaned to remove any foreign contaminants. This step was essential to ensure that the FBG sensors could function at optimal capacity and efficiency. After cleaning, the FBG sensors were carefully positioned on the railway track surface and securely affixed using UV-curable adhesive, as illustrated in Figure 3.

FIGURE 3. FBG sensors with rectangular rosette arrangement at thermite area

DATA GATHERING AND ANALYSIS

Next, the wavelength shift data obtained from the FBG sensors were converted into strain values by dividing the measured wavelength shifts by a sensitivity factor of 1.2 pm/µƐ (Agosmustaram et al. 2024). This conversion enabled the determination of the strain experienced by the railway track under each wheel load at various sensor orientations. A key advantage of using a rosette configuration is its ability to fully characterize the strain tensor. This configuration requires three sensors oriented at distinct angles, allowing strain measurements in three independent directions. As illustrated in Figure 4, the rosette configuration provides three direct strain components: ε_a,ε_b and ε_c. By analyzing these components, both the magnitude and direction of the strain can be precisely determined.

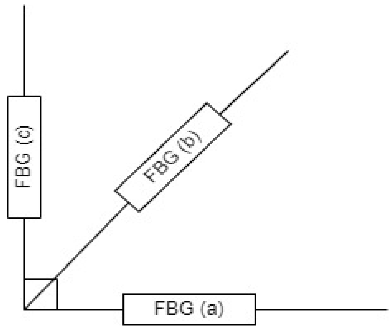

FIGURE 4. FBG Sensors with rectangular rosette arrangement; (a) horizontal 0°, (b) 45°, (c) vertical 90°

To obtain the direct value from arbitrary x- and y-axis-related angles. The cartesian component of the strain has three distinct directions associated ε_{xx}, ε_{yy} and γ_{xy} (C. Mansfield et al. 2020):

$$\varepsilon_a = \varepsilon_{xx}cos^2\theta_a + \epsilon_{yy}sin^2\theta_a + \gamma_{xy}sin\theta_a cos\theta_a \quad (1)$$

$$\varepsilon_b = \varepsilon_{xx}cos^2\theta_b + \epsilon_{yy}sin^2\theta_b + \gamma_{xy}sin\theta_b cos\theta_b \quad (2)$$

$$\varepsilon_c = \varepsilon_{xx}cos^2\theta_c + \epsilon_{yy}sin^2\theta_c + \gamma_{xy}sin\theta_c cos\theta_c \quad (3)$$

where θ is the angle between the x-axis and the directions a, b, and c. The above equation enables the determination of the principal strain as:

$$\varepsilon_{1,2} = \frac{1}{2}\left(\varepsilon_{xx} + \varepsilon_{yy}\right) \pm \frac{1}{2}\left(\left(\varepsilon_{xx} - \varepsilon_{yy}\right)^2 + {\gamma_{xy}}^2\right)^{\frac{1}{2}} \quad (4)$$

The equation of strain will become:

$$\varepsilon_a = \varepsilon_{xx} \qquad (5)$$

$$\varepsilon_b = \frac{1}{2}\left(\varepsilon_{xx} + \varepsilon_{yy} + \gamma_{xy}\right) \qquad (6)$$

$$\varepsilon_c = \varepsilon_{yy} \qquad (7)$$

$$\gamma_{xy} = 2\varepsilon_b - \varepsilon_a - \varepsilon_c \qquad (8)$$

The strain equation may then be substituted into the principal strain equation to produce:

$$\varepsilon_{1,2} = \frac{1}{2}(\varepsilon_a + \varepsilon_b) \pm \frac{1}{2}(\varepsilon_a - \varepsilon_c)^2 + ([2\varepsilon_b - \varepsilon_a - \varepsilon_c]^2)^{\frac{1}{2}} \qquad (9)$$

By incorporating the rectangular strain rosette value into the principal strain equation, it is possible to determine the principal stress that is present in the component:

$$\sigma_{1,2} = E\left[\left\{\frac{\varepsilon_a + \varepsilon_c}{2(1-v)}\right\} \pm \left\{\frac{1}{2(1+v)}([(\varepsilon_a - \varepsilon_c)]^2 + (2\varepsilon_b - \varepsilon_a - \varepsilon_c)^2)^{\frac{1}{2}}\right\}\right] \qquad (10)$$

where v is the material's Poisson ratio and E is its Young's modulus. In this study, the rail grade is R260, with $E = 2.10 \times 10^5$ MPa and $v = 0.25$ (J. Herian et al. 2011).

RESULTS AND DISCUSSIONS

FBG sensors are installed on the railway track to evaluate strain behavior under loading conditions, as illustrated in Figure 5. The vertically oriented sensor (90°) recorded strain indicative of downward deflection, attributed to high compressive forces. The 45° sensor, positioned between the others, exhibited bidirectional strain responses due to the combined effects of tensile and compressive stresses. Meanwhile, the horizontally oriented sensor (0°) captured an upward strain signal, reflecting tensile expansion.

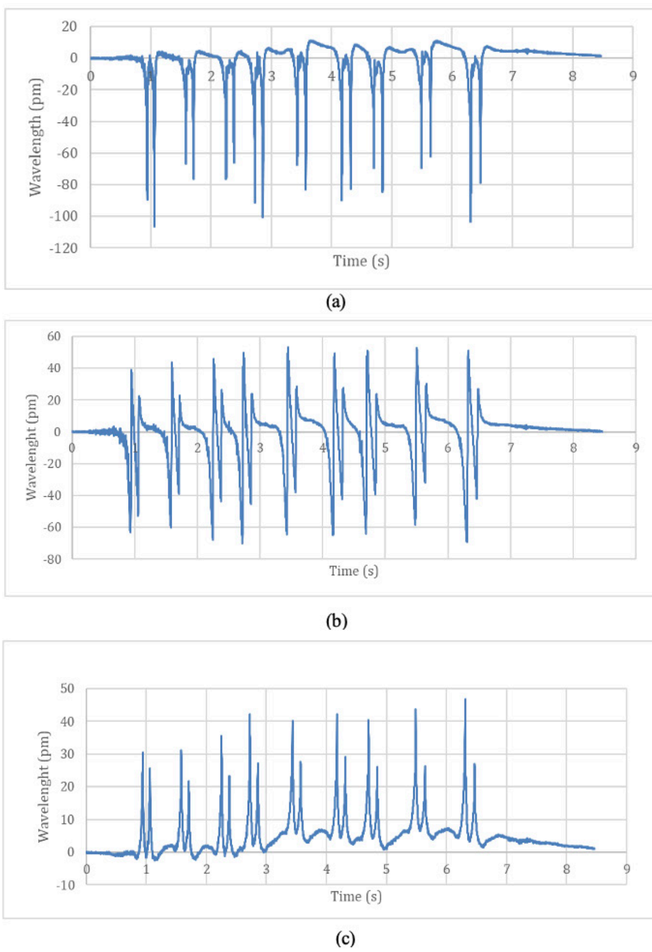

FIGURE 5. (a) Wavelength at 90° direction sensor (b) Wavelength at 45° direction sensor (c) Wavelength at 0° direction sensor

TABLE 1. Shows the results and data gathered from the study

No. wheels	Wavelength 45° (pm)	Wavelength vertical (pm)	Wavelength Horizontal (pm)	Strain 45° (με)	Strain Horizontal (με)	Strain vertical (με)	Principal strain 1 (MPa)	Principal strain 2 (-MPa)	Principal stress 1 (MPa)	Principal stress 2 (MPa)
1	-62.96	-89.39	30.4	-57.23	27.64	-81.26	35.56	89.19	2.9721	17.9872
2	-52.8	-106.5	25.58	-48.0	25.0	-95.0	26.39	96.39	0.5138	20.1138
3	-60.09	-66.25	31.14	-54.62	28.31	-60.59	42.66	74.93	5.3599	14.3966
4	-39.05	-76.57	21.71	-35.49	19.74	-69.61	20.97	70.84	0.7307	14.6951
5	-68.06	-74.99	35.64	-61.87	32.4	-69.47	48.35	85.42	6.0469	16.4267
6	-43.74	-65.45	23.27	-39.75	20.72	-59.5	25.59	64.37	2.1283	12.9872
7	-69.88	-91.19	42.28	-63.52	38.43	-82.9	51.15	95.62	6.1048	18.5544
8	-45.5	-100.17	27.1	-41.36	24.64	-91.57	25.17	92.1	0.482	19.2214
9	-64.54	-67.65	40.11	-58.67	36.46	-60.95	55.04	79.53	7.8764	14.7334
10	-38.25	-82.43	27.02	-34.77	25.12	-74.93	26.08	75.9	1.5921	15.5416
11	-64.83	-89.54	42.26	-58.93	38.41	-81.4	49.15	92.14	5.8508	17.8879
12	-42.02	-82.52	29.18	-38.19	26.53	-75.01	28.41	76.9	2.0584	15.6348
13	-64.18	-69.25	39.58	-58.34	36.75	-62.96	54.21	80.42	7.6405	14.9795
14	-39.35	-84.54	26.05	-35.77	23.68	-77.11	24.49	77.92	1.1224	16.0827
15	-58.25	-69.25	43.79	-52.95	39.8	-62.96	54.39	77.55	7.8424	14.3255
16	-31.77	-61.78	25.7	-28.88	23.93	-56.16	25.91	58.15	2.549	11.5747
17	-69.3	-103.24	46.91	-62.99	42.64	-93.86	52.22	103.43	5.9051	20.2444
18	-42.01	-78.67	27.03	-38.18	24.36	-71.52	26.54	73.7	1.8188	15.0228

The downward signal recorded by the 90° sensor corresponds to significant compression in this orientation. The 45° sensor exhibited both upward and downward deflections, with the dominant downward wavelength averaging -53.14 pm due to prevailing compressive forces. The 0° sensor recorded an average wavelength of 32.49 pm, indicating tensile strain. As an 18-tire train passed over the sensors, strain variations were observed, reflecting the dynamic load distribution.

Table 1 summarizes the average wavelength values: -81.08 pm for the 90° sensor, -53.14 pm for the 45° sensor, and 32.49 pm for the 0° sensor. These results highlight the multidirectional strain behavior of the railway track, emphasizing the effect of sensor orientation on strain distribution under operational loading.

The formula explained in the methodology is used to calculate the data from the rosette configuration with 0°, 45°, and 90° orientations. The results for the principal strain and stress are presented in Table 1. The average value for principal strain 1 is 37.35 με, while principal strain 2 is -81.36 με. The negative value indicates that the sensor experienced a compressive force. The average value for principal stress 1 is 3.81 MPa, and for principal stress 2 is 16.13 MPa.

When a train moves along the rail, several force components can be identified that act on both the track and the train. These forces are generally categorized into three main directions: vertical, longitudinal, and lateral, as illustrated in Figure 6. The vertical forces are primarily due to the weight of the train and dynamic interactions between the wheels and the rails. Longitudinal forces arise from traction and braking actions, while lateral forces result from steering movements and curvature of the track. Each of these force components plays a crucial role in influencing the mechanical behaviour of the rail material. The combined effect of these multidirectional forces can lead to stresses and strains that may cause wear, fatigue, deformation, and, over time, potential structural failure of the rail. Understanding how the rail material responds to these different modes of loading is essential for ensuring the long-term integrity, durability, and safety of the railway infrastructure (Parameters, 2017).

The strain experienced at welded rail joints is primarily caused by the weight of the train as it moves along the track (Wheeler et al. 2018). When a train passes over a welded joint, the vertical load from the train wheels exerts compressive forces on the rail, leading to the development of negative strain values. These negative values indicate that the rail material is undergoing compressive deformation, which, if repeated over time, can lead to material fatigue and potential structural degradation at the welded joints. Such conditions are particularly critical in high-speed rail systems or tracks with heavy axle loads, where stress concentrations are more pronounced.

Lateral forces acting on the rail are mainly generated by the combination of wheel loads and dynamic effects arising from the motion and direction changes of the wheels. These forces become more significant when the train navigates curves or switches tracks, where side thrust is naturally higher. Furthermore, additional lateral forces are introduced through the bending (flexural deformation) and torsion (twisting motion) of the rail, which occur as the rail responds to uneven track geometry, wheel-rail contact irregularities, and sudden load changes. These complex interactions result in fluctuating lateral stresses that affect both the mechanical and structural performance of the rail system.

The vertical instability observed in the strain signal patterns recorded by FBG sensors is often linked to lateral instability at the interface between the wheel and the rail surface (Esmaeili et al. 2017). Such instability may arise from imperfect wheel alignment, rail irregularities, or changes in wheel-rail contact geometry. The sensitivity of FBG sensors allows for the detection of these subtle changes, which manifest in the vertical direction typically oriented at 90° to the rail surface. Both longitudinal and lateral forces can influence the FBG sensor output in this vertical orientation, though their effects differ in magnitude and frequency.

Among the two, longitudinal forces generally produce lower strain values compared to lateral forces. These longitudinal forces are associated with the traction force generated during train acceleration and the braking force during deceleration. As the train slows down, the braking force is transmitted through the wheels to the rails, which can result in a phenomenon known as rail creep (Wu et al. 2021). Rail creep refers to the gradual longitudinal displacement of the rail in the direction of train movement, which can lead to alignment issues and contribute to track degradation over time.

A positive strain value detected by the FBG sensor in the horizontal direction indicates that the rail is undergoing positive deformation, which corresponds to tensile stress. This suggests that the rail material is being stretched along the horizontal axis due to longitudinal forces, such as those induced by traction or braking during train operation. The FBG sensor placed at a 45° angle provides insight into the combined behaviour of strain responses in both the horizontal (0°) and vertical (90°) directions. It captures the resultant effect of multiple force components acting simultaneously on the rail structure, offering a more comprehensive picture of the rail's deformation behaviour under complex loading conditions.

The observed negative strain values are significantly higher in magnitude than the positive strain values. This indicates that the compressive forces acting on the rail, particularly from the vertical and lateral directions, are more dominant than the tensile forces from longitudinal loading. This is largely because the vertical forces generated by the weight of the train and dynamic impacts are much higher than those generated by longitudinal traction or braking. Lateral forces, which arise due to wheel-rail interaction during curving or from imperfections in track geometry, also contribute considerably to the strain state of the rail, especially near joints and curved sections.

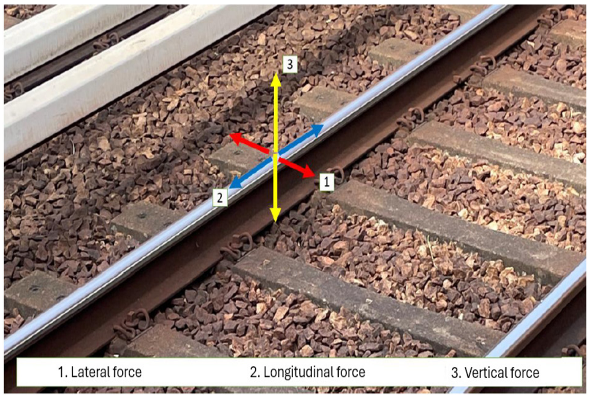

FIGURE 6. Force components on the rail

The vertical direction exhibits much greater strain than the horizontal direction due to the direct transfer of heavy vertical loads from the train wheels to the rail. These loads cause significant compressive deformation in the rail, which is accurately captured by the FBG sensors aligned perpendicularly (90°) to the rail axis. Meanwhile, the FBG sensor at 45° captures the resultant of all three force vectors (vertical, lateral, and longitudinal) and the resulting strain pattern offers a more nuanced view of how the rail responds to multi-axial stress states. This angular sensor orientation is particularly useful in detecting complex deformation behaviours that may not be fully captured by sensors placed strictly along horizontal or vertical axes.

From the strain graph patterns obtained through experimental data, it becomes evident that the 45° sensor reflects a mixed influence of the three primary force components. The deformation behaviour of the rail, as recorded by the FBG sensors, is affected differently by each force component depending on the direction and magnitude of the applied load. Among these, the vertical force remains the most significant, exerting the highest influence on the overall strain behaviour. This dominance is consistent across different load scenarios, such as static loads from stationary trains and dynamic loads during acceleration, deceleration, or vibration.

In summary, the FBG sensor at 90° is most responsive to vertical and lateral forces, as these forces produce larger strain magnitudes in that direction. Conversely, the 0° sensor is primarily affected by longitudinal forces, which result in smaller strain values due to the relatively lower intensity of those forces. The strategic placement of FBG sensors in multiple orientations enables a holistic understanding of the mechanical responses of the rail, supporting the development of improved monitoring systems and predictive maintenance models for railway infrastructure.

CONCLUSION

This study identified three distinct structural responses based on the orientation of FBG sensors mounted on the rail. Each orientation 0°, 45°, and 90° provided unique insight into the deformation characteristics and force interactions within the rail structure. The sensor oriented at 90° recorded the highest compressive strain, averaging -73.69 με, which can be attributed to the direct vertical loading applied by the train wheels. This compressive response reflects the dominant influence of vertical forces acting perpendicular to the rail surface, resulting in significant deformation in this direction.

The sensor positioned at 45° exhibited a bidirectional strain response, registering both compressive and tensile strain components. This mixed behaviour, with an average strain of -48.31 με, indicates the presence of complex force interactions that combine vertical, lateral, and longitudinal loads. The 45° orientation is particularly effective in capturing the resultant of multidirectional loading conditions, which commonly occur during dynamic train movements, such as acceleration, deceleration, and track curvatures.

In contrast, the sensor aligned at 0° recorded only tensile strain, with an average value of 29.40 με. This positive strain signifies that the rail experienced elongation in the longitudinal direction, most likely due to traction forces from wheel movement and thermal expansion. The absence of compressive response at this angle highlights the directional sensitivity of FBG sensors and the effectiveness of using multiple orientations to capture a comprehensive view of the rail's structural behaviour.

Moreover, variations in train speed, axle load, and vibration were found to significantly influence the magnitude and distribution of strain across the different sensor orientations. As the train velocity increases, dynamic loading effects become more pronounced, leading to changes in the wavelength and amplitude of strain signals, especially in the vertical and diagonal orientations. These variations underscore the importance of accounting for operational conditions when interpreting FBG sensor data. The strategic deployment of multiple FBG sensors at varying angles offers substantial benefits in terms of measurement resolution and structural health monitoring. By capturing localized strain responses with high sensitivity and spatial resolution, these sensors enable detailed assessment of stress distribution patterns, early detection of anomalies, and evaluation of fatigue-prone areas in the rail.

ACKNOWLEDGEMENT

The author would like to express her gratitude to the Kementerian Pengajian Tinggi (KPT) Malaysia under research grant FRGS/1/2020/TK02/UKM/03/1 for supporting the research project entitled "Embedded Machine Learning-Based with Continuum Damage Model for Railway Running Rail (RRR) using Optical Strain Measurement" in collaboration with Prasarana Malaysia Berhad.

DECLARATION OF COMPETING INTEREST

None.

REFERENCES

Abuhamdia, T., Taheri, S., Meddah, A., & Davis, D. 2014. Rail defect detection using data from tri-axial accelerometers. *2014 Joint Rail Conference*.

Agosmustaram A.D.H., Ahmad M.I.M, Suhaimi N.S., Nuawi M.Z., Zohari M.H, Ariffin A.K. and Abdullah A.Z.M. 2024. Monitoring for strain-based railway structure assessment approach using optical fibre sensor. *Jurnal Kejuruteraan* 36(2): 793-799.

Ahmad M.I.M, Arifin A. and Abdullah S. 2016. Evaluating effect of magnetic flux leakage signals on fatigue crack growth of mild steel. *Journal of Mechanical Engineering and Sciences (JMES)* 10(1): 1827-1834.

C. Mansfield, M. M., & O'sullivan. 2020. *Understanding Physics*. John Wiley & Sons.

Du, Cong & Dutta, Susom & Kurup, Pradeep & Yu, Tzuyang & Wang, Xingwei. 2020. A Review of railway infrastructure monitoring using fiber optic sensors. *Sensors and Actuators* 303: 111728. 10.1016/j.sna.2019.111728.

Esmaeili, M., Zakeri, J.A. & Babaei, M. 2017. Laboratory and field investigation of the effect of geogrid-reinforced ballast on railway track lateral resistance. *Geotextiles and Geomembranes* 45(2): 23-33.

Falamarzi, Amir & Moridpour, Sara & Nazem, Majidreza. 2019. A review on existing sensors and devices for inspecting railway infrastructure. *Jurnal Kejuruteraan*.

Herian, J. & Aniolek, K. 2011. Modelling of structure and properties of pearlitic steel and abrasive wear of the turnout frog in the cyclic loading conditions. J. Achiev. *Mater. Manuf. Eng.* 49(1): 71–81.

Nordin, N. H., Mohd Masirin, M. I., Ghazali, M. I., & Azis, M. I. 2017. Appraisal on Rail Transit Development: A review on train services and safety. *IOP Conference Series: Materials Science and Engineering*, *226*, 012034.

Oe, T., Nawa, Y., Tsuda, N., & Yamada, J. 2010. Nondestructive internal defect detection using photoacoustic and self-coupling effect. *Electronics and Communications in Japan* 93(7): 17–23.

Parameters, I. 2017. Department of Civil Engineering. *International Research Journal of Engineering and Technology (IRJET)* 4(2): 1-2.

Quan, Yu, Dawei He, Yongsheng Wang, and Pengfei Wang. 2014. Axle Counter for High-Speed Railway Based on Fibre Bragg Grating Sensor and Algorithm Optimization for Peak Searching. 7th International Symposium on Advanced Optical Manufacturing and Testing Technologies: Smart Structures and Materials for Manufacturing and Testing 9285:92850D.

Suhaimi N.S., Ahmad M.I.M., Nuawi M.Z., Zohari M.Z., Ariffin A.K. and Abdullah A.Z.M. 2024a. Determination of train vehicle speed using fibre bragg grating sensors for railway application. *Jurnal Kejuruteraan* 36(2): 785-792.

Suhaimi N.S., Ahmad M.I.M., Nuawi M.Z., Zohari Z.M., Sajuri Z. and Abdullah A.Z.M. 2024b. The effect of railways speed on the rail track structure strain behaviour using fibre optical sensor. *AIP Conf. Proc.* 2998, 050010-1-050010-11.

Suhaimi N.S., Ahmad M.I.M., Nuawi M.Z., Ariffin A.K. and Abdullah A.Z.M. 2023. Structural condition assessment based strain-stress behaviour for railway welded rail joint using rosette fibre bragg grating optical sensor. *Results in Engineering* 19: 101300.

Velha, P., Nannipieri, T., Signorini, A., Morosi, M., Solazzi, M., Barone, F., Frisoli, A., Ricciardi, L., Eusepi, R., Icardi, M., Recchia, G., Lupi, M., Arcoleo, G., Firmi, P., & Di Pasquale, F. 2020. Monitoring large railways infrastructures using hybrid optical fibers sensor systems. *IEEE Transactions on Intelligent Transportation Systems* 21(12): 5177–5188.

Wheeler, L., Take, W.A., Hoult, N.A. & Le, H. 2018. The use of fiber optic sensing to measure distributed rail strains and determine rail seat forces due to a moving train. *Canadian Geotechnical Journal*, 1-42.

Wu, Q., Sun, Y., Spiryagin, M. & Cole, C. 2021. Railway track longitudinal force model. *Vehicle System Dynamics* 59(1): 155-170.

Zhang, Y., Liu, F., Jing, Y. & Li, W. 2017. Application of FBG sensing technique for monitoring and early warning system of high-speed railway track conditions. 2017 *25th Optical Fiber Sensors Conference (OFS)*, pp. 1-4, doi: 10.1117/12.2265412.